Self-Collimation of Light over Millimeter-Scale Distance in a Quasi-Zero-Average-Index Metamaterial

V. Mocella,[1] S. Cabrini,[2] A. S. P. Chang,[2] P. Dardano,[1] L. Moretti,[1] I. Rendina,[1] D. Olynick,[2] B. Harteneck,[2] and S. Dhuey[2]

[1]*CNR-IMM, Unità di Napoli, Via P. Castellino 111, 80131 Napoli, Italy*

[2]*Molecular Foundry, Lawrence Berkeley National Laboratory, Berkeley, California, USA*

(Received 10 September 2008; revised manuscript received 16 February 2009; published 2 April 2009)

Inspired by the concept of complementary media, we experimentally demonstrate that an engineered metamaterial made of alternating, stripe layers of negatively refracting (photonic crystals) and positively refracting (air) materials strongly collimates a beam of near-infrared light. This quasi-zero-average-index metamaterial fully preserves the beam spot size throughout the sample for a light beam traveling through the metamaterial a distance of 2 mm—more than 1000 times the input wavelength $\lambda = 1.55$ μm. These results demonstrate the first explicit experimental verification of optical antimatter as proposed by Pendry and Ramakrishna [J. Pendry and S. Ramakrishna, J. Phys. Condens. Matter **15**, 6345 (2003)], using two complementary media in which each $n_{\text{eff}} = -1$ layer appears to annihilate an equal thickness layer of air.

DOI: 10.1103/PhysRevLett.102.133902 PACS numbers: 42.70.Qs, 78.20.Ci

The advent of Negative Index Materials (NIMs) [1] media for controlling electromagnetic waves has raised the possibility [2–5] of intriguing materials properties unavailable in naturally occurring, positive-index materials. Recent experimental reports have shown the potential of NIMs in imaging [6] and magnifying [7] for superlens applications. However, the self-collimation [8,9] of a propagating beam of light in NIMs that can overcome another fundamentally important effect, diffraction-induced beam spreading, has remained largely unexplored. In particular, negatively refracting dielectric photonic crystals (PhCs) [10,11] represent a viable route for realizing NIMs capable of controlling long-range light propagation due to their low absorption losses. Recently, subdiffraction imaging in the near-infrared was experimentally demonstrated using negatively refracting PhCs, verifying the amplification of evanescent waves in these metamaterials [12]. The use of negatively refracting PhCs for collimation is attractive because in contrast to their positive counterparts, they can accept and capture evanescent light at all angles, making subwavelength beam size and transfer of near-field information conceivable in these materials. Consider a 2D silicon-based PhC with airholes arranged in a hexagonal lattice on a silicon-on-insulator (SOI) wafer. The 1.5 μm silicon layer is on a 1 μm oxide layer, with index contrast at the interfaces providing vertical light confinement. In this case, the silicon thickness is large enough to practically behave as a 2D system. Indeed, the effective index of the fundamental mode supported by a uniform slab of this thickness is indistinguishable from the bulk silicon value for both polarizations ($n_{\text{eff}} = 3.45$ for $\lambda = 1.55$ μm). When the ratio of hole radius r and lattice parameter a is 0.38 at the normalized frequency $\omega_n = 0.305$, the PhC behaves as a medium with effective index $n_{\text{eff}} = -1$ for TM polarization (the electric field directed along the holes axis). For $\lambda = 1.55$, this corresponds to $r = 180$ nm and $a = 472$ nm. In reciprocal space, the EquiFrequency Surface (EFS) represents the locus of propagating wave vectors supported by the unbounded PhC structure. The EFS of such a PhC around ω_n collapses to the origin of the Brillouin zone, as opposed to expanding with increasing frequency as in positively refracting media. The EFS calculated for $\omega_n = 0.305$, Fig. 1(a), essentially has the circular shape of an isotropic medium, whereas the group velocity, $\vec{v}_g = \partial\omega/\partial\vec{k}$, is directed inward, in the opposite direction of the corresponding wave vector, such that $\vec{v}_g \cdot \vec{k} < 0$. Such a PhC acts as an effective negative refractive index medium [10,11]. By repeatedly alternating a striped layer consisting of this PhC with a striped layer of air of equal length, a zero volume-averaged refractive index is obtained. The PhC layer and the air layer in each pair can be regarded conceptually as complementary media-spatial regions that optically cancel each other out, resulting in both of them appearing nonexistent to the incident light [13–15]. In the limit of an extremely small layer length, the negative refraction of the alternating layers can be exploited to collimate a light beam travelling through the metamaterial system [16,17]. Figure 1(b) depicts an ex-

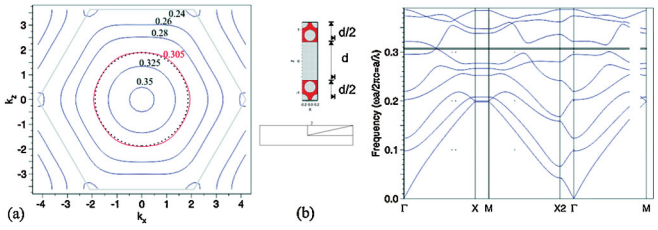

FIG. 1 (color). Negative refraction by a PhC and zero-average-index band gap. (a) The EFSs for TM polarization show a negative $\vec{v}_g$. The dashed circle is the air dispersion curve for $\omega_n = 0.305$ that is practically superposed to the corresponding EFS of the PhC. (b) The band diagram of the supercell, composed of equal lengths of negative refracting PhC and air. The zero-average band gap appears at $\omega_n = 0.305$.

ample of such a periodic supercell structure, obtained by stacking three rows of the hexagonal PhC (i.e., a length of $\sqrt{3}a$ corresponding to one unit cell of the PhC in the z-direction), with an equal length of air. In designing such a heterostructure over a large area using a real metamaterial, it is important to note the lack of impedance matching of the ideal complementary media [13–15]. In general case, for a system of alternating positive and negative index materials, a full photonic bandgap appears whenever an exactly zero-average refractive index is obtained [18,19]. This point is illustrated in the calculated band structure for the supercell [Fig. 1(b)]. At the normalized frequency $\omega_n = 0.305$, where $n_{\mathrm{eff(PhC)}} = -1$, the zero-average index condition is met, but a very narrow photonic bandgap also appears. A time domain calculation of propagation in this structure using a Finite Difference Time Domain (FDTD) code confirms the radiation is completely reflected by the structure at this frequency, in agreement with a zero-average-index band gap. For this reason, the two media, negative PhC and air, cannot be exactly complementary if light transmission through the system is desired. To open up a propagating state through the structure, we create a slight imbalance between the positive and negative components of the heterostructure by slightly modifying the length of each PhC layer, while largely preserving the complementary nature of the PhC/air bilayers. Thus, the zero-average-index condition is modified to close the band gap and allow the propagation of light. It is well known that surface termination is particularly important for subwavelength imaging with negatively refracting PhCs [20–22], as it plays a crucial role in coupling the evanescent component of the incident wave with propagation in the negatively refracting PhC. The reflection properties of PhCs can be substantially modified by surface termination [23] that modifies the surface impedance of the PhC and induces band gap closing. By carefully designing the PhC termination and layer length slightly away from the zero-average-index condition, while matching the energy flux at the PhC interface, transmission of the incident wave is maximized while the coupling of the evanescent component is optimized.

Following such design requirements, we introduce a quasi-zero-average-index (QZAI) heterostructure based on negatively refracting PhC [Fig. 2(a)]. Each PhC stripe has a length of $(3\sqrt{3} - 0.4)a$, corresponding to $0.92a$ in air. The calculated light intensity profile and energy flux illustrate the light beam propagation along the structure from bottom to top [Fig. 2(a)]. The 3×6 μm device area shown is located 10 μm from the front of the heterostructure. The intensity profile, obtained using 2D FDTD calculations with a Gaussian incident beam width of $\lambda/5$ at a half period of the PhC ($1.5\sqrt{3}a$) from the front of the first PhC stripe (not shown) and perfectly matched layer boundary conditions, shows that a well-confined light propagation is established along the heterostructure, with the beam

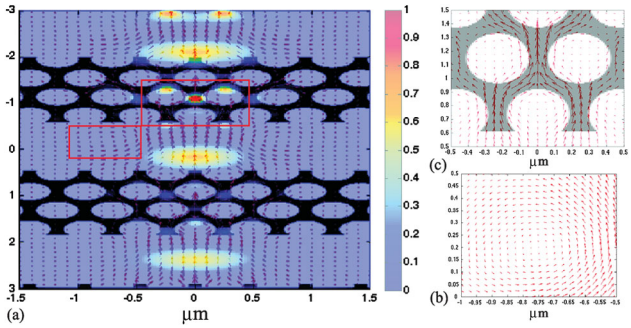

FIG. 2 (color). The field propagating inside the QZAI metamaterials calculated using a FDTD code. (a) The intensity of the electric field component E_y (TM polarization). (b) The time-average Poynting vector. (c) Surface termination helps match the air and negatively refracting PhCs.

spot size preserved 100 μm from the entrance interface. In essence, the beam is refocused in every stripe as it propagates, resulting in a strong macroscopic self-collimation effect over the entire length of the metamaterial. As this air-PhC structure is not exactly balanced (i.e. quasi-zero index), the refocusing at each pair of stripes is not located at the same relative z-position, and the beam shape is not exactly the same after each refocusing. Yet, the beam is well-confined along the structure. This effect does not involve any nonlinearity and can in principle be carried on over large distances.

Looking carefully at the energy flux [Fig. 2(b)], obtained as the time-average of the Poynting vector, we see that optical vortices play a crucial role in coupling the evanescent wave component into the structure. This mechanism was shown previously at the interface of NIM and air [24] and in transmission by subwavelength slits [25], where it is essential to trap light in the vicinity of the aperture to observe enhanced transmission and its related phenomena. Observing energy flux inside a PhC stripe [Fig. 2(c)] gives more insight into the propagation mechanism. An extremely collimated shape is preserved in the absence of any physical waveguide structure that laterally confines the beam.

The 2×2 mm device (Fig. 3) was fabricated on a SOI substrate using a high-precision nanofabrication process

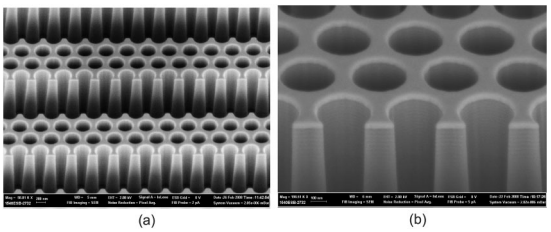

FIG. 3. SEM images of the nanofabricated device. (a) Alternating of space and photonic crystal material, with different termination on each PhC structure. (b) Magnified image.

with high-voltage electron beam lithography and a gas-chopping inductively coupled plasma etching process [26]. Scanning electron microscope (SEM) images of the device shows airholes with a diameter of 360 nm and periodicity of 470 nm in every PhC stripe. The experimental setup for optical characterization of the device [Fig. 4(a)] consisted of a CW laser ($\lambda = 1.55$ μm emission), connected to a lensed input fiber producing an incident full width half maximum (FWHM) beam spot size of 2.9 μm measured experimentally. The input and output fibers are fixed on two different 3-axis nanopositioning stages with a resolution of 20 nm and are used to optimize coupling between the incident beam, as delivered from the lensed fiber, and the PhC heterostructure.

The light propagation inside the heterostructure is directly observed using an IR camera Xenics Xeva 185 and a high numerical aperture (NA = 0.42) objective with a long working distance. Our structures are designed with the requirement $n_{\mathrm{eff(PhC)}} = -1$; i.e., the PhC EFS lies exactly on the air light cone [Fig. 1(a)]. To monitor the light propagation, light scattering out-of-plane (x, z) from the heterostructure is achieved by moving the lensed fiber in the y-direction. This produces a slight misalignment between the input fiber and silicon guiding layer, resulting in a small vertical component for the incident wave that couples with propagating wave vectors in air. Monitoring the scattered radiation takes into account that the metamaterial exhibits a periodic modulation of refractive index in the z-direction due to the alternating air and PhC layers [Fig. 4(b)]. The period Λ of such effective grating profile is given by the distance between two air layers (or two PhC layers), equivalently: $\Lambda = 3\sqrt{3}a = 2.453$ μm. The radiation scattered out-of-plane (x, z) will couple with the mth-order of this grating such that, if $k_i n = 2\pi/\lambda$ is the wave vector in the (x, z) plane, the scattered radiation in (y, z) plane will have components with z-component $k_{z,m} = k_i n + m2\pi/\Lambda$ coupled with the grating periodicity. This is equivalent to the application of the grating equation $m\lambda = \Lambda(\sin\alpha + \sin\beta)$, where the incident wave vector $k_i n$ with respect to the normal forms an angle $\alpha = -90$ and consequently the mth-diffracted orders, with respect to the normal, have angle β: $\sin\beta = 1 + m\lambda\Lambda$ where $m = \pm 1, \pm 2 \ldots$. Among the components of the scattered waves, only three orders propagate. They are associated with orders $m = -1, -2, -3$, for which $|\sin\beta| \leq 1$ is satisfied. An experimental angular scan, performed in the y-z plane Fig. 4(c), clearly shows the diffraction peak located exactly at the angle $\beta = 21.5°$. The angular scan also proves only a small fraction of energy is coupled to grating order whereas the propagating wave, $\beta = 90°$ corresponding to $m = 0$ in grating equation, is two order-of-magnitude larger. The insertion loss is minimized by the surface termination design and are estimated in theory to be less than 0.2 dB. In this experiment, the insertion losses between the entrance of the metamaterial and the input lensed fiber are estimated to be 1.2 dB due to impedance and mode mismatch in the coupling between the structure and the input lensed fiber. IR images of the light beam recorded along $\beta_{-1} = 21.5°$ provide clear evidence of a collimated beam propagating along the entire metamaterial [Fig. 5(a)], with the energy extremely concentrated in comparison to equivalent propagation over unpatterned SOI [Fig. 5(b)] recorded with an input power 2 orders of magnitude larger. Detailed images of the field intensity inside the structure are also recorded. The 20×20 μm images recorded along the propagation direction z [Figs. 5(c)–5(e)] strikingly demonstrate preservation of beam width and strong beam confinement along the entire propagation distance in the x direction, without any structure to laterally limit the beam in this direction. The beam profile is extracted from Figs. 5(c)–5(e) and exhibits a well-confined shape with a FWHM $= 2.9 \pm 0.4$ μm in the first part of the sample, Fig. 5(f) ;FWHM $= 3.2 \pm 0.4$ μm in the middle part, Fig. 5(g); and FWHM $= 3.0 \pm 0.4$ μm at the end of the sample Fig. 5(h).

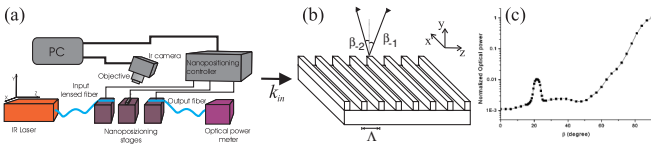

FIG. 4 (color online). Experimental setup and grating coupling. (a) Schematic of experimental setup. (b) Out-of-plane scattering couples with grating direction β_{-1}, β_{-2}. (c) Angular scan in logarithmic scale in the (y, z) plane.

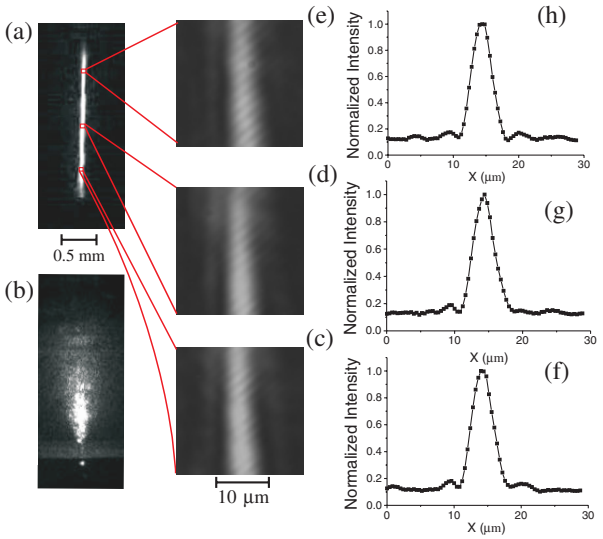

FIG. 5 (color online). The experimental images. (a) The image of the scattered radiation along the β_{-1} direction reveals a well-collimated beam along the whole 2 mm length of the sample, (b) compared to the propagation over the unpatterned SOI. (c) A magnified image of the scattered radiation in the first part, (d) in the middle, and (e) in the final part of the quasi-zero-average metamaterial. (f)–(h) The corresponding beam profile.

Even considering the worst case of Fig. 5(f), the FWHM of the transmitted beam is, within the measurement error, indistinguishable from that of the incident beam. This proves beam spreading is negligible over the entire length of these QZAI metamaterials. Interestingly, in our experiments, the beam intensity is largely preserved throughout the device, suggesting vertical diffraction from the device is low. Furthermore, the experimental results are consistent with the theoretical predictions.

We are aware that this structure cannot totally fulfill the requirements for an ideal complementary media as described in [13]. It is clear that PhCs can be considered negatively refracting media in the sense of an effective medium description [10,11]. Finally, the finite size of the PhC structure as compared with the wavelength limits the recovery of all evanescent components of the incident beam, i.e., arbitrarily small details of the source at the image plane and ideal complementary behavior is affected from the impedance mismatch between air and PhC [27]. A negative index metamaterial based on a purely dielectric photonic crystal has slightly smaller lattice period compared to a metallodielectric fishnet metamaterial operating in the same wavelength range and exhibiting a large figure of merit between the real and imaginary parts of the refractive index [1]. Taking into account such limitations, our simulation shows that subwavelength spot size can be obtained for the collimated beam over a large scale, whereas previous experiments have already verified the amplification of evanescent components by a single slab of a very similar PhC metamaterial [12]. These results provide for the possibility of supercollimation at subwavelength beam spot size and efficient long-range spatial transfer of near-field information. These findings could impact a wide range of applications, such as imaging and optical interconnect systems. What's more, these results imply the synergistic combination of negative- and positive-index materials could lead to greatly enhanced versatility and flexibility, potentially resulting in a variety of new devices and systems unachievable in negative-only or positive-only media. For example, functional elements could be incorporated in the positive-index portion of the metamaterial; the negative and positive portions can be individually designed and optimized, adding extra degrees of freedom to the design. On a more fundamental level, the results presented here can be regarded as a first explicit experimental verification of the concept of optical antimatter [13]. For the frequency where the condition $n_{\text{eff}} = -1$ is satisfied, a slab of metamaterial appears to annihilate an equal thickness slab of air. Neither in air nor in metamaterial does the light follow a straight line, as shown in Fig. 2(a), but the global effect is as if a 2 mm space was optically removed and becomes invisible to the specific wavelength.

Portions of this work were performed at the Molecular Foundry, Lawrence Berkeley National Laboratory, which is supported by the Office of Science, Office of Basic Energy Sciences, of the U.S. Department of Energy under Contract No. DE-AC0205CH11231.

[1] V. Shalaev, Nat. Photon. **1**, 41 (2007).
[2] J. Pendry, Phys. Rev. Lett. **85**, 3966 (2000).
[3] U. Leonhardt, Science **312**, 1777 (2006).
[4] J. Pendry, D. Schurig, and D. Smith, Science **312**, 1780 (2006).
[5] K. Tsakamakidis, A. Boardman, and O. Hess, Nature (London) **450**, 397 (2007).
[6] N. Fang, H. Lee, C. Sun, and X. Zhang, Science **308**, 534 (2005).
[7] I. Smolyaninov, Y.-J. Hung, and C. Davis, Science **315**, 1699 (2007).
[8] P. Rakich, M. Dahlem, S. Tandon, M. Ibanescu, M. Soljac, G. Petrich, J. Joannopoulos, L. A. Kolodziejski, and E. P. Ippen, Nature Mater. **5**, 93 (2006).
[9] Z. Lu, S. Shi, J. Murakowski, G. Schneider, C. Schuetz, and D. Prather, Phys. Rev. Lett. **96**, 173902 (2006).
[10] M. Notomi, Phys. Rev. B **62**, 10696 (2000).
[11] M. Notomi, Opt. Quantum Electron. **34**, 133 (2002).
[12] R. Chatterjee, N. Panoiu, K. Liu, Z. Dios, M. Yu, M. Doan, L. Kaufman, R. Osgood, and C. Wong, Phys. Rev. Lett. **100**, 187401 (2008).
[13] J. Pendry and S. Ramakrishna, J. Phys. Condens. Matter **15**, 6345 (2003).
[14] J. Pendry, Contemp. Phys. **45**, 191 (2004).
[15] S. Ramakrishna, Rep. Prog. Phys. **68**, 449 (2005).
[16] E. Shamonina, V. Kalinin, K. Ringhofer, and L. Solymar, Electron. Lett. **37**, 1243 (2001).
[17] S. A. Ramakrishna, J. Pendry, M. Wiltshire, and W. Stewart, J. Mod. Opt. **50**, 1419 (2003).
[18] J. Li, L. Zhou, C. Chan, and P. Sheng, Phys. Rev. Lett. **90**, 083901 (2003).
[19] N. Panoiu, R. Osgood, S. Zhang, and S. Brueck, J. Opt. Soc. Am. B **23**, 506 (2006).
[20] S. Xiao, M. Qiu, Z. Ruan, and S. He, Appl. Phys. Lett. **85**, 4269 (2004).
[21] X. Zhang, Phys. Rev. B **71**, 165116 (2005).
[22] A. Martinez and J. Marti, Phys. Rev. B **71**, 235115 (2005).
[23] V. Mocella, P. Dardano, L. Moretti, and I. Rendina, Opt. Express **15**, 6605 (2007).
[24] K. Webb and M. Yang, Phys. Rev. E **74**, 016601 (2006).
[25] H. Schouten, T. Visser, D. Lenstra, and H. Blok, Phys. Rev. E **67**, 036608 (2003).
[26] D. Olynick, A. Liddle, and I. Rangelow, J. Vac. Sci. Technol. B **23**, 2073 (2005).
[27] S. A. Ramakrishna, S. Guenneau, S. Enoch, G. Tayeb, and B. Gralak, Phys. Rev. A **75**, 063830 (2007).